

pubs.acs.org/JACS Article

# Optical Cavity Manipulation and Nonlinear UV Molecular Spectroscopy of Conical Intersections in Pyrazine

Daeheum Cho,\* Bing Gu,\* and Shaul Mukamel\*



Cite This: J. Am. Chem. Soc. 2022, 144, 7758–7767



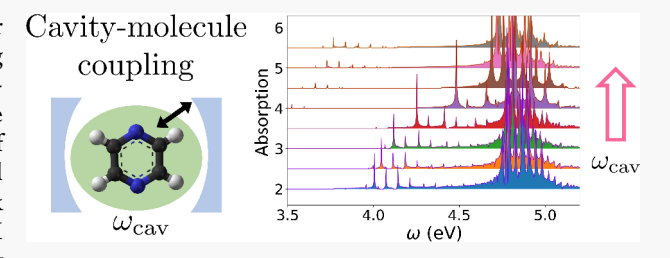
**ACCESS** I

Metrics & More

Article Recommendations

Supporting Information

ABSTRACT: Optical cavities provide a versatile platform for manipulating the excited-state dynamics of molecules via strong light—matter coupling. We employ optical absorption and two-multidimensional electronic spectroscopy simulations to investigate the effect of optical cavity coupling in the nonadiabatic dynamics of photoexcited pyrazine. We observe the emergence of a novel polaritonic conical intersection (PCI) between the electronic dark state and photonic surfaces as the cavity frequency is tuned. The PCI could significantly change the nonadiabatic dynamics of pyrazine by



doubling the decay rate constant of the  $S_2$  state population. Moreover, the absorption spectrum and excited-state dynamics could be systematically manipulated by tuning the strong light-matter interaction, e.g., the cavity frequency and cavity coupling strength. We propose that a tunable optical cavity-molecule system may provide promising approaches for manipulating the photophysical properties of molecules.

# INTRODUCTION

Optical cavities provide a novel means for controlling the photochemistry and photophysics of molecules by making use of strong light–matter coupling without chemical modifications or strong external laser pulses. Optical cavities are standing-wave light resonators that can be made of high-reflectivity mirrors (Fabry–Perot type), photonic crystals, nanomaterials, or microcircuits. The coupling can be created between electronic transitions of embedded molecules and the confined cavity photon mode with the strength  $g=\mu\sqrt{N}\sqrt{\frac{\hbar\omega_c}{2V\epsilon_0}}$  where  $\mu$  is the transition dipole,  $\epsilon_0$  is the

electric permittivity of a vacuum, N is the number of molecules in the cavity mode, which is in the vacuum state, V is volume, and  $\omega_c$  is the cavity frequency. The effective coupling strength can be enhanced by increasing the molecular concentration N/V. The electronic and optical properties of molecules<sup>2,19</sup> are affected by vacuum fluctuations of the cavity mode. The Purcell effect, which increases the spontaneous emission rates of atoms when placed in a resonant cavity, is a notable result.<sup>23</sup> When the coupling strength is greater than the loss rate of the cavity mode and the decoherence rate of the molecule, the strong light-matter coupling regime is realized. The electronic or vibrational molecular degrees of freedom then combine with the cavity photon to form polaritons, which are of hybrid light-matter states. The ultrastrong coupling regime can be reached in the collective strong coupling regime with many molecules, 3,6,22,24-27 where the coupling strength is comparable to the cavity frequency  $g/\omega_c \approx 0.1-0.2^{.15,28}$  Singlemolecule strong coupling has been reported in plasmonic

nanocavities where  $g \approx 100$  meV and  $\omega_c \approx 1.88$  eV.<sup>29</sup> In the single-excitation space, one major difference between manymolecule and single-molecule strong coupling is that there is a manifold of collective dark states for  $N \gg 1$ , which may affect the cavity-controlled chemical reactions.<sup>30</sup> The splitting of a single molecular resonance into a doublet of polariton states in the absorption and cavity transmission spectra<sup>3</sup> is a signature of strong coupling. However, for a dense electronic state manifold, it is possible to observe only a single polariton state.<sup>31</sup> Cavity polaritons have been shown to strongly affect the electronic, optical, and chemical properties of molecules and materials, such as increasing the conductivity of organic semiconductors, 32 reversing the selectivity of a ground-state chemical reaction,<sup>33</sup> improving optical nonlinearity,<sup>6</sup> and enabling long-range electronic and vibrational energy transfer. 27,34 These findings triggered intense theoretical studies. 1,2,19,35-39

Herein, we investigate cavity effects on molecules undergoing conical intersections. Conical intersections (CIs) in bare molecules play an important role in many chemical and biophysical processes, including the primary event of vision and photostability of DNA molecules, <sup>40</sup> by providing an ultrafast nonradiative electronic decay channel for excited

Received: January 24, 2022 Published: April 11, 2022





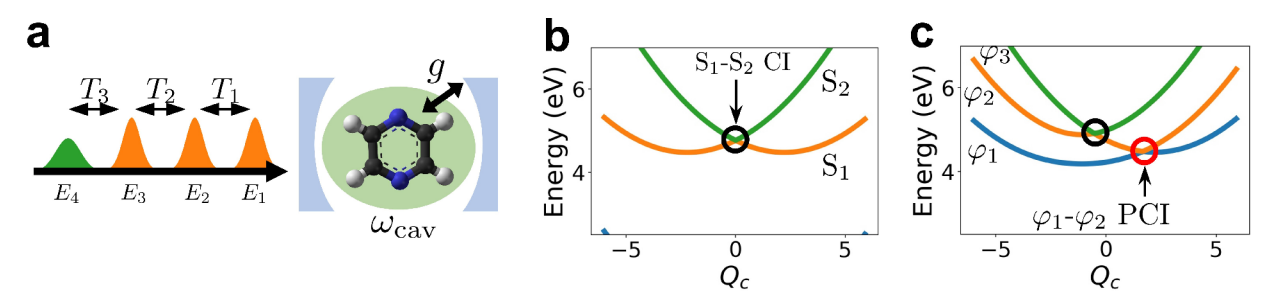


Figure 1. (a) Pulse configuration and time delays for four-wave mixing of a pyrazine molecule in a cavity, (b) 1D adiabatic electronic PES S<sub>n</sub> of the bright  $(S_2)$  and the dark  $(S_1)$  excited states of a bare molecule along the  $Q_c$  vibrational coordinate while  $Q_t$  is fixed at -3.5 where the conical intersection occurs (the electronic ground state  $(S_0)$  is not shown). The black dark circle denotes the CI between the two excited states  $(S_1-S_2 \text{ CI})$ is marked by a black circle. (c) Example of 1D PPESs  $\varphi_n$  of a molecule in a cavity with cavity frequency  $\omega_{\text{cav}} = 4.0 \text{ eV}$  and cavity coupling strength g= 2000 cm<sup>-1</sup>. The red circle denotes the novel PCI ( $\varphi_1 - \varphi_2$  PCI).

molecules due to the strong electron-nuclear coupling at the crossing region. The detection and control of nonadiabatic dynamics around CIs have been extensively studied. 41-47 Various nonlinear spectroscopic techniques have been used to investigate photochemical dynamics around CIs, including monitoring state population dynamics, 48,49 transient vibrational/visible spectra, 50-53 transient absorption, photoionization spectra, 54 and (off-)resonant stimulated X-ray Raman techniques. 55 Nonadiabatic molecular dynamics occur in an optical cavity on polaritonic potential energy surfaces (PPESs), with hybrid electron-photon polaritonic states replacing the bare adiabatic potential energy surfaces. The PPESs have more features than their bare adiabatic counterparts, such as lightinduced crossings and polaritonic conical intersections, 20,86,57 which can be modulated by cavity frequencies and the cavitymolecule coupling. Cavities could significantly alter the photochemistry of molecules and can be used to control photochemical reactions by molecular polaritons. Timeresolved nonlinear spectroscopic techniques are required for the real-time monitoring of ultrafast polaritonic dynamics. 58,59 Experiments in two-dimensional (2D) infrared spectroscopy have been carried out to study the relaxation dynamics of vibrational polaritons.<sup>58,60</sup>

We use multidimensional electronic spectroscopy to investigate the polaritonic dynamics of a pyrazine molecule coupled to a single cavity mode in this study. 2D electronic spectroscopy (2DES) provides a time-resolved ultrafast probe for dynamics in a wide variety of materials, including molecular aggregates and photosynthetic complexes. 61 We previously simulated the polaritonic dynamics and pump-probe transient absorption spectra of a single and a pair of pyrazine molecules in an optical cavity 20,21 and demonstrated that the cavity mode could split the pristine S<sub>1</sub>/S<sub>2</sub> CI into two polaritonic CIs, significantly altering the internal conversion dynamics. The competition between wavepacket dynamics on the bright PPESs and dark-state surfaces determines the polaritonic dynamics of a pair of pyrazines. To monitor polaritonic dynamics in real time, multidimensional electronic spectroscopy of the polaritonic conical intersection should be useful.<sup>21</sup>

To simulate the 2DES of molecules in an optical cavity, we use a phase-cycling protocol in conjunction with a nonadiabatic wavepacket dynamics method. This method avoids diagonalizing the full photon-electron-nuclear Hamiltonian, which is required in perturbative simulations, and also accounts for the pulse shape without employing the impulsive limit. It entails explicitly propagating the polaritonic dynamics including the external probing laser pulses and scanning the

interpulse temporal delays, i.e., coherence time  $T_1$ , population time  $T_2$ , and detection time  $T_3$  (see Figure 1). Polaritonic dynamics is simulated by numerically exact nonadiabatic wavepacket dynamics with two vibrational modes. The phase-cycling protocol dissects the desired third-order response functions, each represented by a Liouville space pathway. 62 We investigate the optical signatures of strong coupling in the nonadiabatic polariton dynamics of photoexcited pyrazine by examining the population dynamics, PPESs, linear absorption, and photon echo spectroscopy. Our simulations demonstrate how the couplings between molecular degrees of freedom (vibrational or electronic) can be extracted from multidimensional spectroscopy by exploiting multiple electric fields.

# THEORY AND COMPUTATIONAL DETAILS

Nonadiabatic Dynamics in an Optical Cavity. The Hamiltonian of a molecule in the optical cavity is given by the sum of the molecular Hamiltonian  $H_{M\nu}$  the cavity photon Hamiltonian  $H_{C}$ , the cavity-matter interaction  $H_{CM}$ , and the classical light-matter interaction  $H_{LM}(t)$ 

$$H = H_{\rm M} + H_{\rm C} + H_{\rm CM} + H_{\rm LM}(t) \tag{1}$$

Pyrazine is modeled by a linear-vibronic coupling effective Hamiltonian developed in ref 63, which includes three electronic states  $(S_0, S_1, \text{ and } S_2)$  and two vibrational modes that are strongly coupled to the electronic system. The ultrafast nonradiative decay is caused by a CI between S1 and S2. This model has been widely used to study the nonadiabatic dynamics via the CI. 40,64 The molecular Hamiltonian in the diabatic basis reads

$$H_{\rm M} = \sum_{k=0,1,2} h_k |\psi_k\rangle \langle \psi_k| + \lambda Q_{\rm c}(|\psi_1\rangle \langle \psi_2| + \text{H.c.})$$
 (2)

where  $h_k = \sum_{\sigma=t,c} \hbar \Omega_{\sigma} (a_{\sigma}^{\dagger} a_{\sigma} + 1/2) + E_k + \kappa_k Q_t$  and H.c. denotes the Hermitian conjugate. Here,  $\Omega_{\sigma}$  and  $Q_{\sigma}$  denote the frequency and dimensionless coordinate of the  $\sigma$ th vibrational mode ( $\sigma = c$  for the coupling mode and  $\sigma = t$  for the tuning mode), respectively,  $|\psi_{\iota}\rangle$  are the diabatic electronic states,  $E_{\iota}$  is its vertical excitation energy at the Franck-Condon point,  $\kappa_k$ are the intrastate electron-vibrational coupling constants, and  $\lambda$  denotes the interstate coupling strength. The parameters used for  $H_{\rm M}$  are  $\hbar\omega_{\rm c}=118$  meV,  $\hbar\omega_{\rm t}=74$  meV,  $E_1=3.94$  eV,  $E_2 = 4.84 \text{ eV}, \ \kappa_1 = -105 \text{ meV}, \ \kappa_2 = 149 \text{ meV}, \ \text{and} \ \lambda = 261.6$ meV. The cavity Hamiltonian is given by

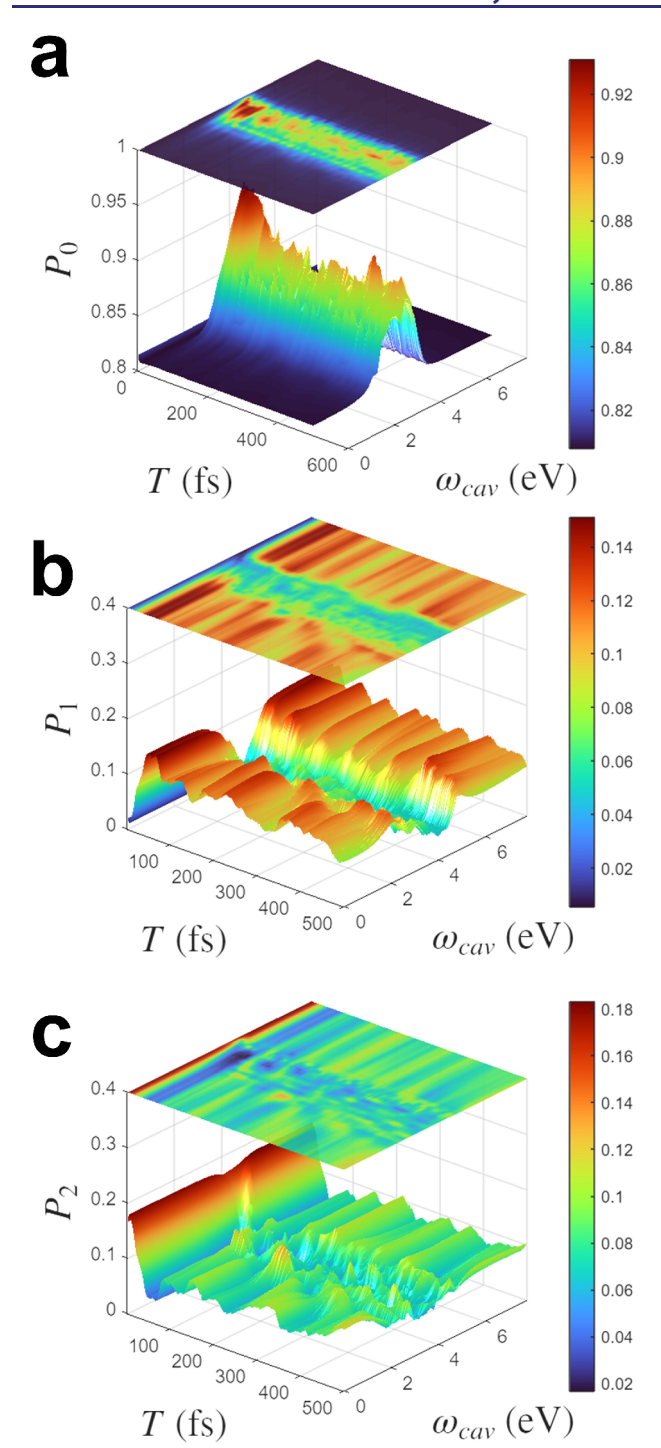


Figure 2. Nonadiabatic polaritonic dynamics for pyrazine coupled to a cavity mode with cavity photon coupling strength  $g = 2000 \text{ cm}^{-1}$ . Population dynamics of electronic states (a)  $\psi_0$  (S<sub>0</sub>), (b)  $\psi_1$  (S<sub>1</sub>), and (c)  $\psi_2$  (S<sub>2</sub>) as functions of the time delay T and the cavity frequency  $\omega_{\rm cav}$ . The initial decay of  $P_0$  and the initial preparation of  $P_2$  are not shown for better visibility.

$$H_{\rm C} = \hbar \omega_{\rm cav} (a_{\rm cav}^{\dagger} a_{\rm cav} + 1/2) \tag{3}$$

where  $\omega_{cav}$  denotes the resonance frequency of the single cavity mode and  $a_{cav}$  ( $a_{cav}^{\dagger}$ ) denotes the annihilation (creation) operator of the cavity photon.

The cavity-molecule dipole interaction is

$$H_{\rm CM} = \sum_{i < j} g_{ij}(\mathbf{R}) (a_{\rm cav}^{\dagger} + a_{\rm cav}) (|\psi_j\rangle \langle \psi_i| + \text{H.c.})$$
(4)

where  $g_{ii}$  is the coupling strength and  $\mathbf{R} = (Q_t, Q_c)$  denotes nuclear coordinates. We use the Condon approximation because the transition dipole moment matrix elements between diabatic states have a negligible dependence on the nuclear coordinates.

The nonadiabatic dynamics of pyrazine in the optical cavity are precisely simulated by numerically solving the timedependent Schrödinger equation with a complete basis set of the full polaritonic space. A polaritonic basis function is a direct product of the diabatic electronic state  $|\psi_k\rangle$ , the cavity mode Fock state  $|n_{cav}\rangle$ , and the Fock states for the two vibrational modes  $|n_c\rangle \otimes |n_t\rangle$ , i.e.,  $|kn_{\rm cav}n_cn_t\rangle = |\psi_k\rangle \otimes |n_{\rm cav}\rangle \otimes$  $|n_c\rangle \otimes |n_t\rangle$  The basis set used in all simulations is  $n_e = 3$ ,  $n_{cav} =$ 2, and  $n_t = n_c = 20$ , resulting in a total of 2400 basis functions in the polaritonic space. The Runge-Kutta fourth-order method was used to integrate the time-dependent Schrödinger equation for the joint light-molecule system with a time step of  $\delta t = 0.04$  fs. The resulting states were used to calculate the time-dependent polarization  $\langle \mu(t) \rangle$ , and the phase-cycling protocol was used to obtain the 2DES signal.

Phase-Cycling Protocol for Four-Wave Mixing Signals. Nonlinear optical signals are given by sums over Liouville pathways, representing different orders in the fields. To isolate the desired nonlinear signal, direct time-domain simulation of multidimensional signals of molecules driven by external fields requires a phase-cycling protocol. 65-68 While phase-matching is a common method for distinguishing different nonlinear pathways in experiments using noncollinear pulse configurations, phase cycling is a convenient experimental and computational alternative. We employed a nine-step phasecycling protocol to separate the third-order photon echo contribution from the total nonadiabatic dynamics driven by three external UV pulses (refer to Supporting Information for

In third-order nonlinear four-wave mixing (FWM) spectroscopy, the system interacts with three electric pulses  $E_1$ ,  $E_2$ , and  $\mathbf{E}_3$  and is finally detected by the local oscillator field  $\mathbf{E}_4$ , which interferes with the emitted signal to generate the heterodyne signal.

$$S = \Im \int dt \langle \boldsymbol{\mu}(t) \rangle \cdot \mathbf{E}_{4}^{*}(t)$$
 (5)

The third-order signal is given by

$$S^{(3)}(t_3, t_2, t_1) = \int dt dt_3 dt_2 dt_1 R^{(3)}(t_3, t_2, t_1)$$

$$\times \mathbf{E}_4(t) \mathbf{E}_3(t - t_3) \mathbf{E}_2(t - t_3 - t_2) \mathbf{E}_1(t - t_3 - t_2 - t_1)$$
(6)

The third-order response function  $R^{(3)}(t_3, t_2, t_1)$  can be expanded in Liouville pathways (see Supporting Information Figure S1 for diagrams).

$$R^{(3)}(t_3, t_2, t_1) = \sum_{n=1}^{6} R_n(t_3, t_2, t_1) + \text{c.c.}$$
(7)

The 2D photon echo signal  $S(\Omega_1, T_2, \Omega_3)$  is displayed by a double Fourier transform of the third-order photon echo polarization  $P(T_1, T_2, T_3)$  with respect to the pulse delays  $T_1$ and  $T_3$  as follows:

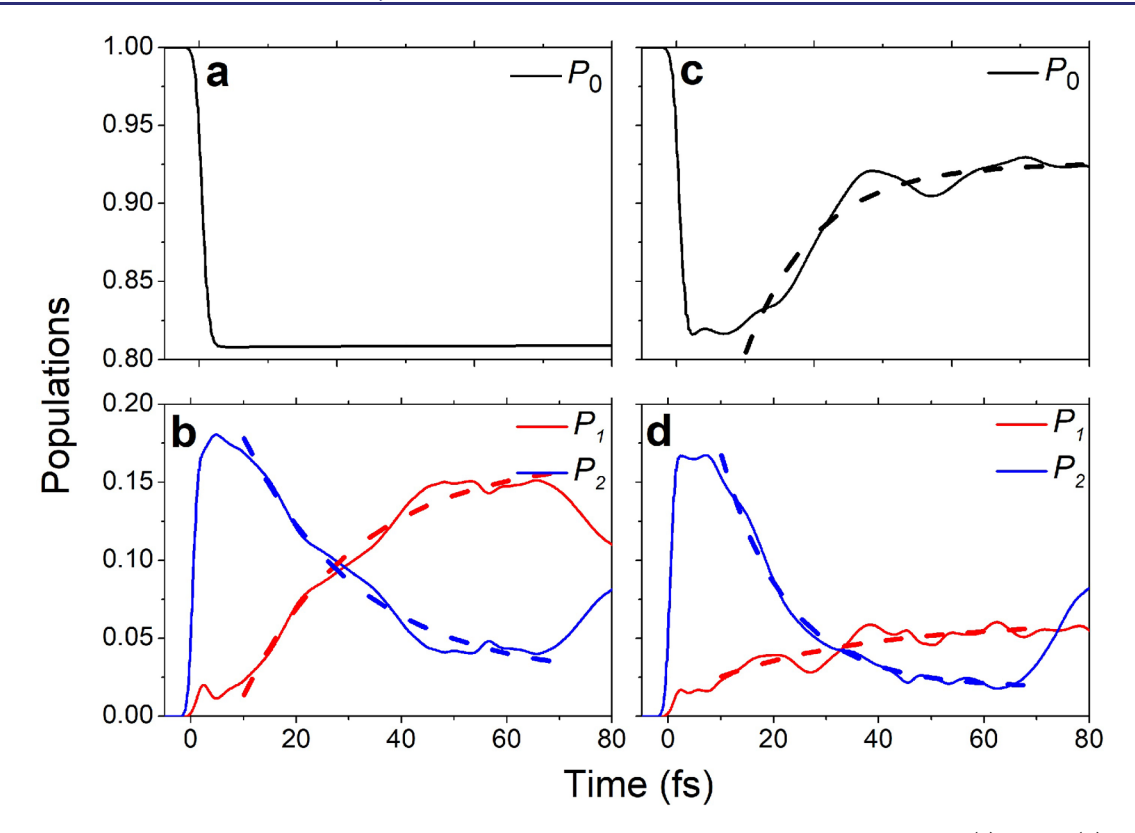


Figure 3. 1D cuts of the population dynamics of electronic states shown in Figure 2 at different cavity frequencies. (a)  $P_0$  and (b)  $P_1$  and  $P_2$  of a bare molecule. (c)  $P_0$  and (d)  $P_1$  and  $P_2$  of a molecule coupled to a cavity with  $\omega_{cav} = 4$  eV. Solid (dashed) line represents raw data (exponential fitting of fast decay after initial preparation).

$$S(\Omega_1, T_2, \Omega_3) = \int dT_1 \int dT_3 e^{i\Omega_1 T_1 + i\Omega_3 T_3} S(T_1, T_2, T_3)$$
 (8)

To generate the 2DES spectra shown in Figure 7, we used 1000 sets of wavepacket dynamics with different time delays  $T_1$  and  $T_3$ , each consisting of a simulation time of 2200 fs and a time step  $\Delta t = 0.1$  au. The 2D FWM signals were generated by scanning the delays  $T_1$  and  $T_3$ , with  $T_2 = 10$  and 500 fs.  $T_1$  was varied from 9.0 fs to 501.0 fs in 0.4 fs increments, and  $T_3$  was scanned from 9.0 fs to 1001.0 fs in 0.4 fs increments. We assumed the Gaussian electric field envelopes as follows:

$$\mathbf{E}_{i}(t) = A \sin(\omega_{i}(t - t_{i}) + \phi_{i}) \exp[-(t - t_{i})^{2}/(2\sigma_{i}^{2})]$$
 (9)

with an electric field strength of A=0.01 au  $(3.51\times 10^{14} \text{ W/cm}^2)$  for all incoming fields, central time  $t_i$ , central frequency  $\omega_i$ , pulse duration  $\sigma_i$ , and phase  $\phi_i$ . Time delays between pulses are given by  $T_i=t_{i+1}-t_i$ . The pulse central frequencies were set to  $\omega_1=4.7$  eV and  $\omega_2=\omega_3=\omega_4=4.0$  eV with pulse durations of 10 fs at full-width at half-maximum (fwhm).

#### RESULTS AND DISCUSSION

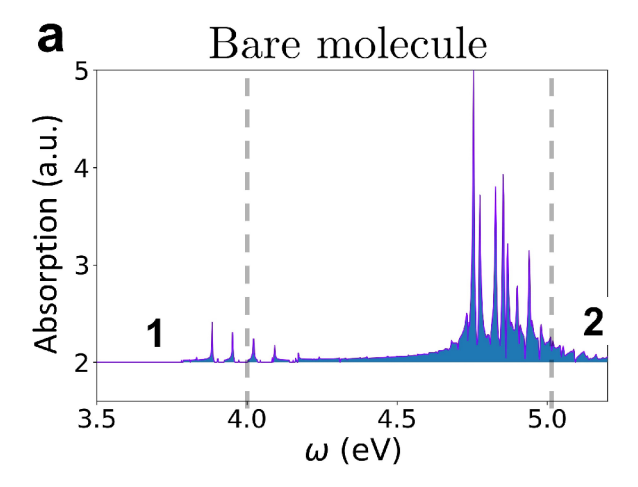
**Dynamics and the Absorption Spectrum.** The population dynamics of adiabatic electronic states and the absorption spectra of pyrazine driven by a single electric field

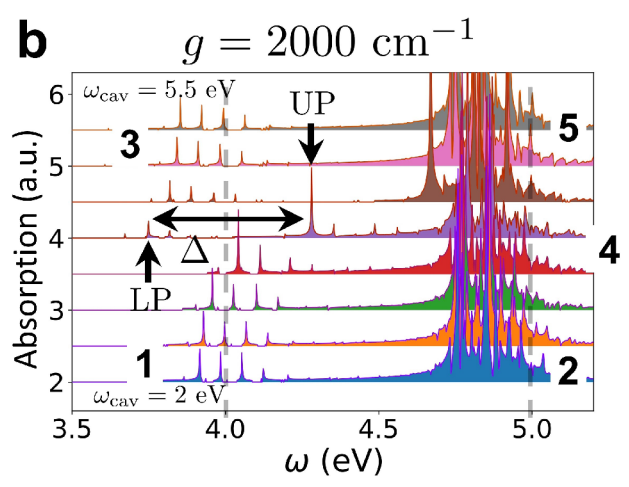
Table 1. Fitting Parameters for the Early Population Dynamics to an Exponential of the Form  $y = a_1e^{-kx} + y_0$ 

	$P_{1,\mathrm{bare}}$	$P_{2,\mathrm{bare}}$	$P_{0,\mathrm{cav}}$	$P_{1,\mathrm{cav}}$	$P_{2,\mathrm{cav}}$
k	0.045	0.045	0.097	0.034	0.080
а	-0.241	0.243	-0.322	-0.050	0.333

 $\mathbf{E}_1$  with a central frequency  $\omega_1 = 4.7$  eV are first discussed. Previously, the nonadiabatic dynamics of a pyrazine molecule in a cavity, as well as its transient absorption spectroscopy, were investigated.<sup>20</sup> We begin by scanning the cavity frequency  $\omega_{\rm cav}$  at various coupling strengths (g) to investigate the effect of the light-matter interaction. The electronic states  $\psi_0$  (S<sub>0</sub>),  $\psi_1$  (S<sub>1</sub>), and  $\psi_2$  (S<sub>2</sub>) populations are plotted against the cavity frequency  $\omega_{cav} = [0, 8]$  eV at the cavity-photon coupling strength  $g = 2000 \text{ cm}^{-1}$  in Figure 2. In the bare molecule (g = 0)cm<sup>-1</sup>), the  $S_2$  electronic population  $(P_2)$  grows within 10 fs of initial excitation and further decays to  $S_1$  via the  $S_1$ – $S_2$  CI. The initial decay of the bright excited state population  $P_2$  is fast ( $\sim$ 60 fs). At long times,  $P_2$  and  $P_1$  remain around 0.1 with several recurrences. The limited number of vibrational modes in the model Hamiltonian does not account for the further decay of the S2 population to the S1 surface, and the longertime decay is accentuated by including the additional modes. Because there is no decay channel from  $S_1/S_2$  to  $S_0$ , the electronic population of So does not change during the nonadiabatic dynamics.

The coupling to the cavity photon mode significantly affects the population dynamics. Most importantly, at  $\omega_{\rm cav}\approx 4$  eV, which can couple  $S_0$  and  $S_1$  states via the cavity mode, the  $S_0$  population increases significantly during nonadiabatic dynamics, as shown in Figure 2a, indicating a population transfer from  $S_1$  and  $S_2$  states. The cavity—molecule coupling generates a new polaritonic conical intersection (PCI) that serves as a nonadiabatic transition channel from  $S_1$  to  $S_0$ . The PCI depicted in Figure 5 will be discussed further below. The decrease in the  $S_1$  and  $S_2$  populations for the cavity frequency  $\omega_{\rm cav}=4$  eV (Figure 2b and c) indicates that a significant  $S_1$  population is transferred to  $S_0$  during the nonadiabatic





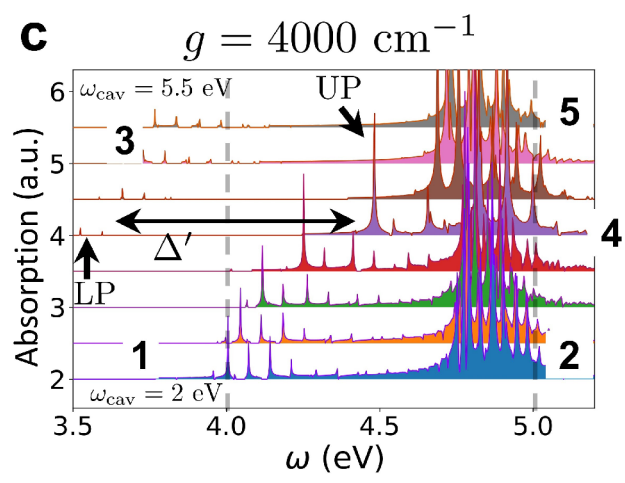


**Figure 4.** Absorption spectra of pyrazine (eq 5). (a) Bare molecule. A molecule in a cavity with different cavity frequencies  $\omega_{\text{cav}} = [2, 5.5]$  with 0.5 eV increments at cavity photon coupling strengths (b)  $g = 2000 \text{ cm}^{-1}$  and (c)  $g = 4000 \text{ cm}^{-1}$ .  $S_1$ ,  $S_2$ , and the PCI bands are marked as 1, 2, and 3, respectively. A blue-shift and a disappearance of the  $S_1$  band are marked as 4. The appearance of a new  $S_1$  band is marked as 5. The  $S_1$  band splits into upper (UP) and lower polariton (LP) modes.

dynamics. Off-resonant cavity modes with the  $S_0$ – $S_1$  gap still produce a noticeable change in the  $S_1$  and  $S_2$  populations. This will be discussed in greater detail in the later text.

The early population dynamics are fitted to provide a quantitative analysis of the polaritonic effects. 1D cuts of  $S_0$ ,  $S_1$ ,

and S2 populations of a bare molecule and a molecule coupled to a cavity with  $\omega_{\rm cav}$  = 4 eV are fitted to an exponential function of the form  $y = a_1 e^{-kx} + y_0$  as shown in Figure 3.  $P_{n,\text{bare(cav)}}$  denotes a population at the  $S_n$  surface of a bare molecule (a molecule coupled to a cavity). Table 1 collects the fitting parameters k and a. Population transfer from  $S_2$  to  $S_1$  in a bare molecule was found from the similar k values for  $P_{1,\text{bare}}$ (0.045) and  $P_{2,\text{bare}}$  (0.045) and opposite sign of a (-0.241) and 0.243) as shown in panels a and b. In a molecule coupled to a cavity (panels c and d), P<sub>2,cav</sub> decays faster and to greater extent than in a bare molecule with k = 0.080 and a = 0.333, while  $P_{1,\text{cav}}$  increases slower and to smaller extent with k = 0.034 and a = -0.050. Importantly, it was found that a molecule—cavity coupling with  $\omega_{cav}$  = 4 eV doubled the rate constant of an early decay of the  $P_{2,cav}$  population. The  $P_{0,cav}$  population rapidly increases with k = 0.097 and a = -0.322 as  $P_{2,cav}$  decreases.

Figure 4 shows the simulated absorption spectra of a bare molecule and a molecule coupled to a cavity mode with cavity frequency  $\omega_{cav} = [2, 5.5]$  eV at g = 2000 and 4000 cm<sup>-1</sup>. Cavity modes with  $\omega_{\rm cav}$  < 2 eV and  $\omega_{\rm cav}$  > 5.5 eV (not shown) do not change the absorption spectra significantly. In panel b, strong peaks originating from the  $S_0 \rightarrow S_2$  transition appear in the 4.7-5.1 eV regime in a bare molecule (denoted as an S<sub>2</sub> band marked as 2). The S<sub>1</sub> band denotes weaker 3.8-4.2 eV peaks originating from the  $S_0 \rightarrow S_1$  transition (marked as 1). Peak 2 is much stronger than peak 1 because the S2 state is a bright state. Nonadiabatic effects result in a fine structure that reveals the propagation of the wavepacket and the vibrational progression on top of the electronic transitions. The fine structure in the S2 band is more complex, whereas the fine structure in the S<sub>1</sub> band is simpler, indicating vibrational wavepackets along a single mode on the S<sub>1</sub> surface. When a pyrazine molecule is coupled to a cavity mode with g = 2000cm<sup>-1</sup> (panel b), we see interesting new features as the cavity frequency  $\omega_{cav}$  increases: the  $S_1$  absorption gradually blue-shifts as the cavity frequency increases from 3.0 to 4.5 eV and eventually merges with the S2 band. At the S1 absorption, another set of peaks appears (marked 3). When a cavity frequency  $\omega_{\rm cav}$  = 4 eV is resonant to the  $\psi_0 - \psi_1$  energy gap, a splitting ( $\Delta$ ) of the S<sub>1</sub> band into two polaritonic modes, upper (UP) and lower (LP) polaritons, is observed. We observe a larger splitting  $(\Delta')$  when the cavity-molecule coupling strength is increased to  $g = 4000 \text{ cm}^{-1}$  (panel c). Besides that, we clearly see the peak shifts induced by the off-resonant (when  $\omega_{cav} \neq 4$  eV) optical cavities.

The PPESs were then used to analyze the spectral features seen in Figure 4. The effect of the cavity-molecule coupling in PPESs is depicted in Figure 5. Figure 5I depicts a 3D plot of PPESs, while Figure 5II and III depict 1D cuts of PPESs along  $Q_c$  at  $Q_t = 0$  and -3.5, respectively. The  $S_1 - S_2$  CI in a bare molecule is located at  $(Q_c, Q_t) = (0.0, -3.5)$ . The wavepacket that was initially promoted to the  $S_2$  state at  $(Q_c, Q_t) = (0.0,$ 0.0) travels to the  $S_1$ – $S_2$  CI to relax to the  $S_1$  surface. The ground  $(\varphi_0)$  and the first excited  $(\varphi_1)$  polaritonic surfaces for the low cavity frequency  $\omega_{cav} = 2$  eV shown in Figure 5b are primarily caused by the coupling between a cavity mode and the electronic ground state. The states  $\varphi_0$  and  $\varphi_1$  have electronic and photonic characters, respectively. The electronic  $S_1$  and  $S_2$  characters dominate the second  $(\varphi_2)$  and the third  $(\phi_3)$  excited polaritonic surfaces, respectively. However, there is no conical intersection between the  $\varphi_1$  and  $\varphi_2$ . Only the S<sub>1</sub>- $S_2$  CI, which can also be called  $\varphi_2 - \varphi_3$  CI, but its character is

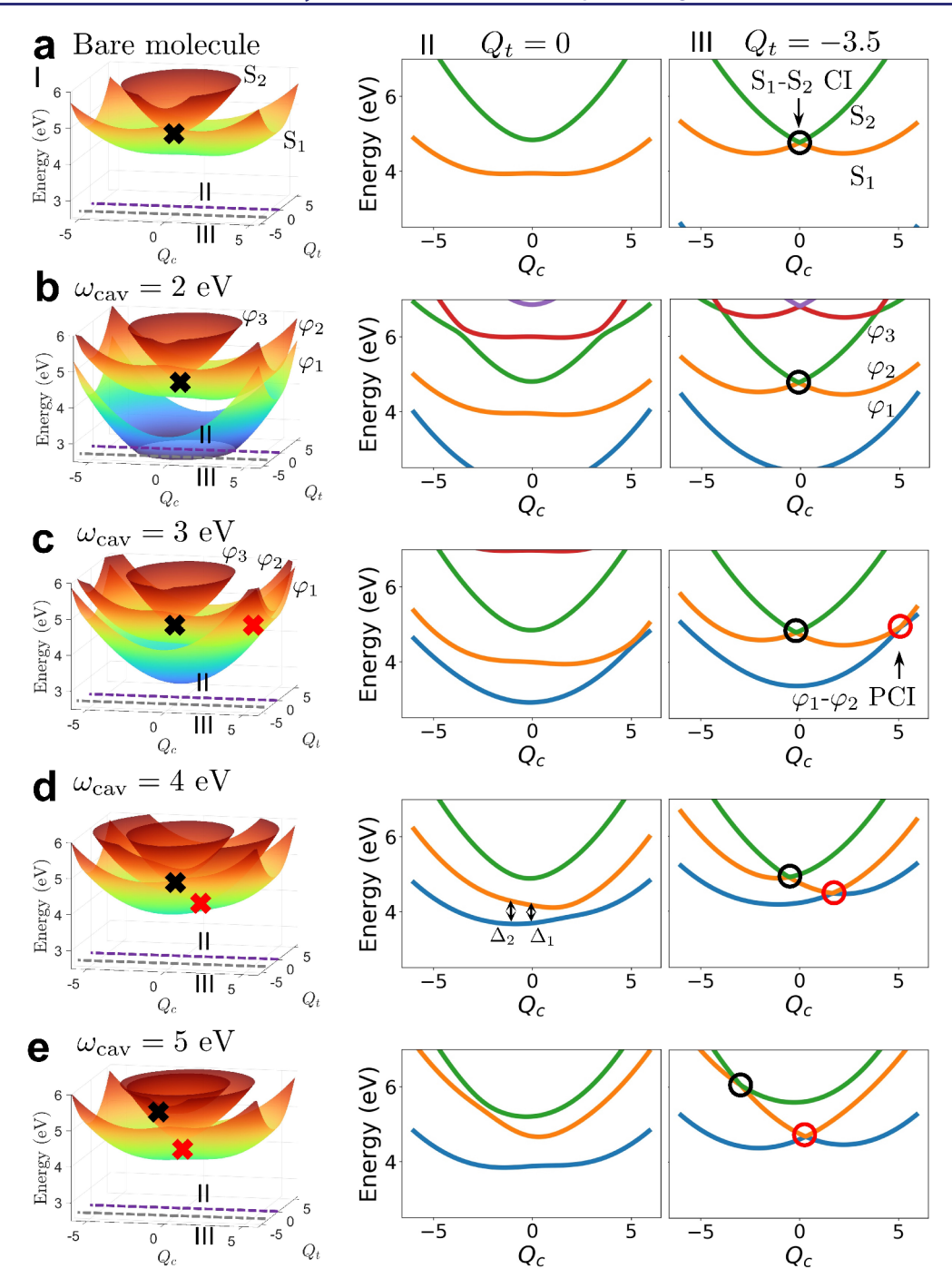
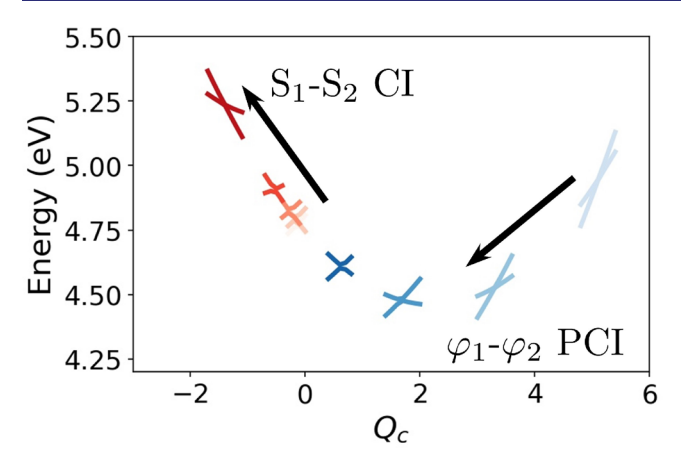


Figure 5. (a) Electronic PES of a bare molecule and (b–e) polaritonic PES (PPES) along the two vibrational coordinates ( $Q_c$  and  $Q_t$ ) at  $\omega_{cav}$  from 2 to 5 eV (at  $g=2000~{\rm cm}^{-1}$ ) (left panel, I) 3D plot of the PESs. 1D cuts of the PPES along  $Q_c$  at (middle panel, II)  $Q_t=0$  and (right panel, III)  $Q_t=-3.5$ . A  $S_1-S_2$  CI and a  $\varphi_1-\varphi_2$  polaritonic CI (PCI) are marked by black and red circles, respectively. In panel e, the  $S_1-S_2$  CI becomes also a polaritonic CI. Higher lying polaritonic surfaces that originated from the light–matter interaction between the cavity photon mode and  $S_1$  and  $S_2$  surfaces are shown in (bII) and (bIII).

the conical intersections between  $S_1$  and  $S_2$ , can be found at  $(Q_c, Q_t) = (0.0, -3.6)$ .

When  $\omega_{\rm cav}$  is increased, the  $\varphi_1$  surface blue-shifts along with the  $\varphi_2$  and  $\varphi_3$  surfaces. This results in a blue-shift in the  $S_1$  band, which is labeled 1 in Figure 4. At  $\omega_{\rm cav}=3$  eV, a new PCI is formed between the  $\varphi_1$  and  $\varphi_2$  surfaces at  $(Q_{c}, Q_t)=(5.1, -3.5)$ , while keeping the location of  $S_1-S_2$  CI at  $(Q_{c}, Q_t)=(-0.6, -3.5)$ . As the PCI is formed, a nonadiabatic electronic transition from  $\varphi_2$  to  $\varphi_1$  occurs, resulting in the new PCI band at  $\omega=3.8$  eV when 4.0 eV >  $\omega_{\rm cav}$ , as shown in Figure 4 marked

as 3. The PCI band is only visible at  $\omega_{\rm cav}=3$  eV because the wavepacket on the  $\varphi_2$  surface cannot reach the  $\varphi_1-\varphi_2$  PCI, which is located at a higher energy than the relaxed minimum of the  $\varphi_2$  surface. The blue-shift of the PCI band at 4.0 eV <  $\omega_{\rm cav}<5.5$  eV indicates that as  $\omega_{\rm cav}$  increases, the  $\varphi_1$  surface shifts to higher energy. The observation of these features experimentally may provide direct evidence for the formation of a PCI via molecule—cavity coupling. As the cavity frequency  $\omega_{\rm cav}$  increases to 5 eV, the  $\varphi_1-\varphi_2$  PCI shifts to  $Q_{\rm c}=0$  and the S<sub>1</sub>–S<sub>2</sub> CI shifts to  $(Q_{\rm c}, Q_{\rm t})=(-4.5, -3.5)$ . As shown in



**Figure 6.** Change in the location of the CI (PCI) as  $\omega_{\rm cav}$  varies from 3.0 eV (light color) to 4.5 eV (deep color) at 0.5 eV increments (at  $g=2000~{\rm cm}^{-1}$ ).  $S_1-S_2$  CIs and  $\varphi_1-\varphi_2$  PCI are colored in red and blue, respectively. Lines represent the shapes of the PPES in the vicinity of the CIs. Black arrows indicate the increase of  $\omega_{\rm cav}$ .

Supporting Information Figure S2, the locations of the  $S_1$ – $S_2$  CI and  $\varphi_1$ – $\varphi_2$  PCI do not change in the  $Q_t$  coordinate.

Figure 6 depicts the shift in the location of the  $S_1$ – $S_2$  CI and  $\varphi_1$ – $\varphi_2$  PCI as the  $\omega_{cav}$  increases from 3.0 to 4.5 eV. The CI and PCI shift along the diabatic  $B_{2u}(\pi\pi^*)$  state as the other diabatic polaritonic surfaces shift to blue because of the cavity–molecule coupling, while the  $B_{2u}(\pi\pi^*)$  surface remains unchanged.

2D Photon Echo Signal of Pyrazine in a Cavity. The 2D photon echo spectra of the bare molecule are compared to those of a molecule coupled to a cavity mode with  $\omega_{cav} = 4 \text{ eV}$ at  $g = 2000 \text{ cm}^{-1}$  in Figure 7. 2D signals of bare pyrazine were calculated earlier for similar models. 69-71 This figure also shows the population transfer during the  $T_2$  delay, which is varied between  $T_2 = 10$  and 500 fs. The spectra were obtained by using the phase cycling protocol described in the section Computational Details in the Supporting Information. The wavepacket detected during the  $T_1$  ( $T_3$ ) time delays causes absorption along the  $\Omega_1$  ( $\Omega_3$ ) axis in the 2D spectra. The 2D spectrum of the bare pyrazine molecule is shown in panel (ai). Key signatures are denoted as S<sub>1</sub> and S<sub>2</sub> bands. The diagonal peaks at  $(\Omega_1, \Omega_3) = (-4.8, 4.8)$  eV and (-3.7, 3.7) eV are signatures of the wavepacket created by the initial excitation from  $S_0$  to  $S_2$  and  $S_1$ , respectively, which remained on the same surface during  $T_1$  and  $T_3$ . Because the transition dipole of the  $S_0 \rightarrow S_1$  transition is smaller than that of the  $S_0 \rightarrow S_2$  transition, the  $(\Omega_1, \Omega_3) = (-3.7, 3.7)$  eV peak is much weaker than that of the (-4.8, 4.8) eV peak. The cross-peaks at  $(\Omega_1, \Omega_3)$  = (-4.8, 3.7) eV correspond to a wavepacket that is initially promoted from S<sub>0</sub> to S<sub>2</sub> and then decays to S<sub>1</sub>. As a result, it provides a signature of the nonadiabatic transition via the conical intersection between  $S_1$  and  $S_2$ . The  $(\Omega_1, \Omega_3) = (-4.8, \Omega_3)$ 3.0) cross-peaks result from the wavepacket initially created at  $S_2$  and transferred to the  $S_1$  surface at  $(Q_t, Q_c) = (-3.5, \pm 2.4)$ through the  $S_1$ – $S_2$  CI (see Figure 5aIII for the PES). This peak reveals the wavepacket traveling from the  $S_1-S_2$  CI to the bottom of the  $S_1$  surface at  $(Q_t, Q_c) = (0.0, \pm 2.2)$  (see Figure 5aII), which is critical information to determine the population transfer during the dynamics. As the wavepacket fully relaxes to the bottom of the  $S_1$  surface, the peak at  $(\Omega_1, \Omega_3) = (-4.8,$ 3.0) diminishes and the peak at  $(\Omega_1, \Omega_3) = (-4.8, 3.7)$ intensifies as shown in panel (bi).

When a molecule is coupled to a cavity mode, a splitting of the  $S_1$  band into UP and LP in the 2D spectra is observed in panel (bi). Two slightly different splittings can be observed from the 2D spectra,  $\Delta_1$  and  $\Delta_2$ , which are the splittings along the  $\Omega_1$  and  $\Omega_3$  coordinates, respectively. As shown in Figure 5dii, the  $\Delta_1$  and  $\Delta_2$  gaps are manifestations of the  $\varphi_1$ – $\varphi_2$  gap at the initial absorption occurring at  $(Q_t, Q_c) = (0.0, 0.0)$  and relaxed wavepackets at the bottom of the  $\varphi_1$  surface  $(Q_t, Q_c) = (0.0, -1.0)$ , respectively.

The population transfer during the nonadiabatic dynamics is reveled by the time delay  $T_2$  dependence of the 2D photon echo signal  $S(\Omega_1, T_2, \Omega_3)$ . When the two signals  $S(\Omega_1, T_2 = 10 \text{ fs}, \Omega_3)$  and  $S(\Omega_1, T_2 = 500 \text{ fs}, \Omega_3)$  are compared, it is discovered that the  $S_1$  band at  $S(\Omega_1, \Omega_3) = S(-4.8, 3.8)$  is significantly enhanced as the population transfers from the  $S_2$  to  $S_1$  surface. Simultaneously, the band at  $S_2$  diminishes as the population transfer nears completion at  $S_2$  diminishes as the population transfer nears completion at  $S_2$  diminishes be and di).

The zoomed-in, black boxed region in Figure 7 highlights the time evolution of the wavepacket that was initially prepared on the  $S_2$  surface. Wavepackets transferring from  $S_2$  to  $S_1(1^{(\prime)})$ , wavepackets on  $S_1(2^{(\prime)})$ , and wavepackets transferring from  $\varphi_2$  to  $\varphi_1(3^{(\prime)})$  are marked as key features. As the population time  $T_2$  is increased, region 2 grows as 1 diminishes in a bare molecule (panels aii and bii), whereas region 2' grows as 3' diminishes in a molecule in a cavity (panels cii and dii). The fine structure created by the vibrational progression at region  $2^{(\prime)}$  intensifies as  $T_2$  increases. As  $T_2$  changes from 10 to 500 fs, the 2D signal intensity of the peaks  $2^{(\prime)}$  and  $3^{(\prime)}$  decreased by 40% as the electronic coherences are lost.

We observed valuable extra information from the 2D spectra as compared to the 1D spectra such as population transfer during the dynamics, relaxation of the excited wavepacket on the PPESs, a splitting between polaritonic states, and how a molecule—cavity coupling manipulates the nonadiabatic dynamics. These insights can be used to design and analyze a cavity-modified photochemistry of a system.

# CONCLUSIONS

We used the phase-cycling protocol in conjunction with quantum wavepacket dynamics to investigate the effect of optical cavity coupling in the nonadiabatic dynamics of photoexcited pyrazine by computing population dynamics, PPESs, the absorption spectrum, and photon echo signals at different cavity-molecule coupling parameter regimes. We observe the emergence of a novel PCI between the electronic and photonic surfaces as the cavity frequency is tuned. The absorption spectra and third-order photon echo signals capture the formation of a novel PCI and its signatures in the polaritonic dynamics. An experimental observation of these spectral features should provide direct evidence of the formation of the PCI. Other spectroscopic signals including photonic decay, vibrational relaxation, and electronic decoherence can be simulated using our computational protocol. For many molecules, the PCIs also occur in the collective polaritonic surfaces, as illustrated for the case of two molecules.<sup>21</sup> Nevertheless, there are complications due to the collective dark states. The collective dynamics will be determined by the competition between nuclear dynamics on the polaritonic surfaces and relaxation to the dark states.<sup>35</sup>

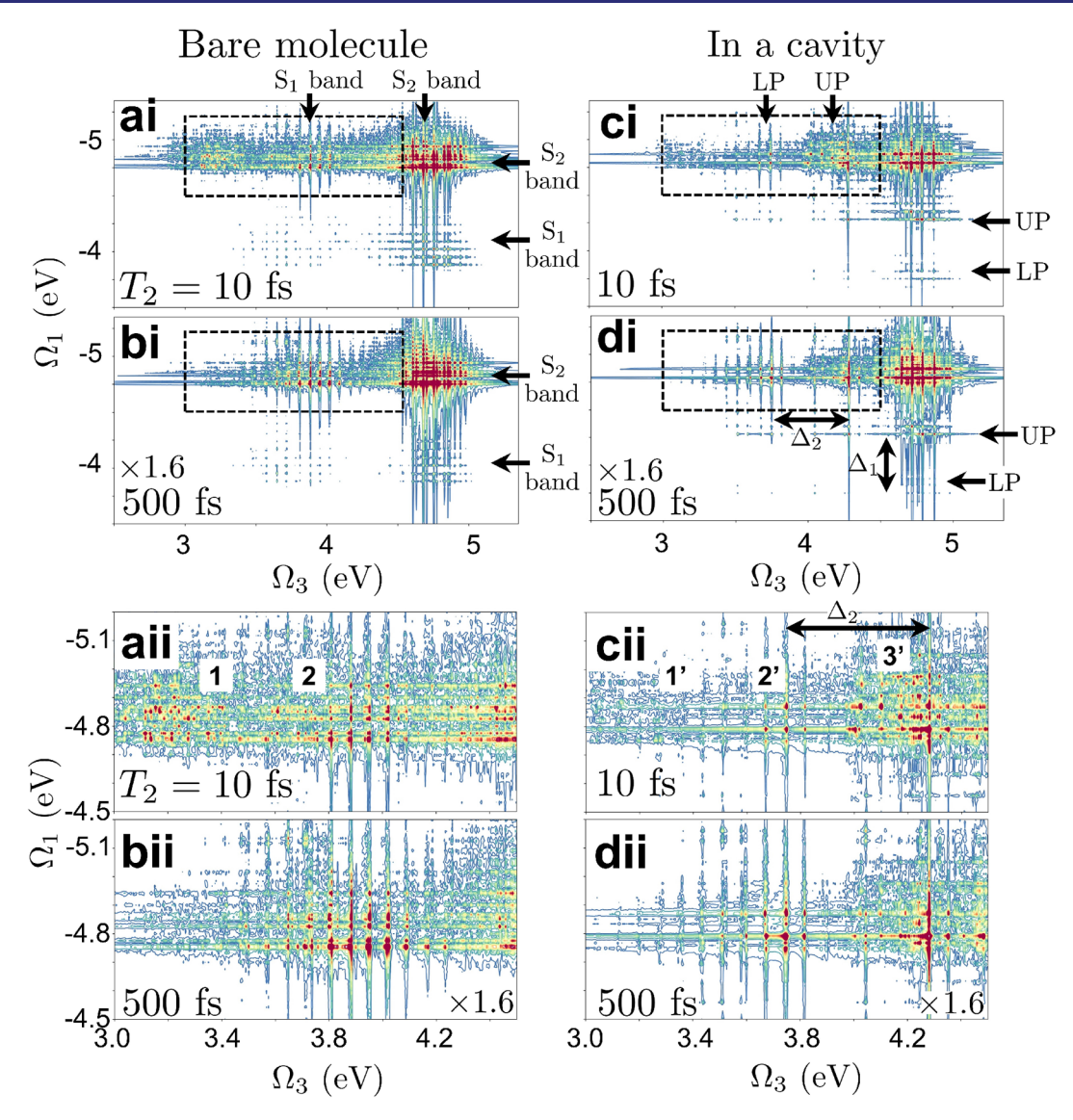


Figure 7. (ai-di) Simulated 2D photon echo spectra  $S(\Omega_1, T_2, \Omega_3)$  (eq 8) of (left) a bare molecule and (right) a molecule in a cavity mode with  $\omega_{\text{cav}} = 4 \text{ eV}$  and coupling strength  $g = 2000 \text{ cm}^{-1}$ . The spectra are simulated at (top)  $T_2 = 10 \text{ fs}$  and (bottom)  $T_2 = 500 \text{ fs}$ .  $S_1$  and  $S_2$  bands are marked. The  $S_1$  band splits into upper (UP) and lower polariton (LP) modes. Separations due to the molecule—cavity coupling ( $\Delta_1$  and  $\Delta_2$ ) are clearly visible when compared to the bare molecule case. (aii-dii) Zoomed-in view of the black-boxed region, which amplifies the time evolution of the wavepacket initially prepared on the  $S_2$  surface. Key regions are marked as  $1^{(r)}$ ,  $2^{(r)}$ , and  $3^{(r)}$ .

# ASSOCIATED CONTENT

#### Supporting Information

The Supporting Information is available free of charge at https://pubs.acs.org/doi/10.1021/jacs.2c00921.

- (1) Phase cycling protocol for four-wave mixing signals;
- (2) supplementary figure for the energy gap between electronic (polaritonic) surfaces along the two vibrational coordinates (Figure S2) (PDF)

#### AUTHOR INFORMATION

#### **Corresponding Authors**

Daeheum Cho – Department of Chemistry and Green-Nano Materials Research Center, Kyungpook National University, Daegu 41566, South Korea; orcid.org/0000-0002-0322-4291; Email: daeheumc@knu.ac.kr

Bing Gu – Department of Chemistry and Physics and Astronomy, University of California, Irvine, California 92697-2025, *United States*; o orcid.org/0000-0002-5787-3334; Email: bingg@uci.edu

Shaul Mukamel — Department of Chemistry and Physics and Astronomy, University of California, Irvine, California 92697-2025, United States; ocid.org/0000-0002-6015-3135; Email: smukamel@uci.edu

Complete contact information is available at: https://pubs.acs.org/10.1021/jacs.2c00921

#### Notes

The authors declare no competing financial interest.

# ACKNOWLEDGMENTS

The support of the National Science Foundation (Grant No CHE-1953045) and the Chemical Sciences, Geosciences, and Biosciences division, Office of Basic Energy Sciences, Office of Science, U.S. Department of Energy, through Award Nos. DE-FG02-04ER15571 (S.M.) and DE-SC0022134 (B.G.), is

gratefully acknowledged. This work was supported by the National Research Foundation of Korea (NRF) grant funded by the Korea government (MSIT) (No. 2021R1C1C2007977). This work was supported by the National Supercomputing Center with supercomputing resources including technical support (KSC-2021-CRE-0187) (D.C.).

# REFERENCES

- (1) Kowalewski, M.; Bennett, K.; Mukamel, S. Cavity Femtochemistry: Manipulating Nonadiabatic Dynamics at Avoided Crossings. *J. Phys. Chem. Lett.* **2016**, *7*, 2050.
- (2) Bennett, K.; Kowalewski, M.; Mukamel, S. Novel Photochemistry of Molecular Polaritons in Optical Cavities. *Faraday Discuss.* **2016**, 194, 259–282.
- (3) Ebbesen, T. W. Hybrid Light-Matter States in a Molecular and Material Science Perspective. Acc. Chem. Res. 2016, 49, 2403-2412.
- (4) Schäfer, C.; Ruggenthaler, M.; Appel, H.; Rubio, A. Modification of Excitation and Charge Transfer in Cavity Quantum-Electrodynamical Chemistry. *Proc. Natl. Acad. Sci. U.S.A.* **2019**, *116*, 4883–4892.
- (5) Galego, J.; Garcia-Vidal, F. J.; Feist, J. Cavity-Induced Modifications of Molecular Structure in the Strong-Coupling Regime. *Phys. Rev. X* **2015**, *5*, No. 041022.
- (6) Shalabney, A.; George, J.; Hutchison, J.; Pupillo, G.; Genet, C.; Ebbesen, T. W. Coherent Coupling of Molecular Resonators with a Microcavity Mode. *Nat. Commun.* **2015**, *6*, 5981.
- (7) Flick, J.; Narang, P. Cavity-Correlated Electron-Nuclear Dynamics from First Principles. *Phys. Rev. Lett.* **2018**, *121*, 113002.
- (8) Herrera, F.; Spano, F. C. Cavity-Controlled Chemistry in Molecular Ensembles. *Phys. Rev. Lett.* **2016**, *116*, 238301.
- (9) Coles, D. M.; Somaschi, N.; Michetti, P.; Clark, C.; Lagoudakis, P. G.; Savvidis, P. G.; Lidzey, D. G. Polariton-Mediated Energy Transfer between Organic Dyes in a Strongly Coupled Optical Microcavity. *Nat. Mater.* **2014**, *13*, 712–719.
- (10) Frisk Kockum, A.; Miranowicz, A.; De Liberato, S.; Savasta, S.; Nori, F. Ultrastrong Coupling between Light and Matter. *Nat. Rev. Phys.* **2019**, *1*, 19–40.
- (11) Vasa, P.; Lienau, C. Strong Light-Matter Interaction in Quantum Emitter/Metal Hybrid Nanostructures. *ACS Photonics* **2018**, *5*, 2–23.
- (12) Hertzog, M.; Wang, M.; Mony, J.; Börjesson, K. Strong Light—Matter Interactions: A New Direction within Chemistry. *Chem. Soc. Rev.* **2019**, *48*, 937–961.
- (13) Hutchison, J. A.; Schwartz, T.; Genet, C.; Devaux, E.; Ebbesen, T. W. Modifying Chemical Landscapes by Coupling to Vacuum Fields. *Angew. Chem., Int. Ed.* **2012**, *51*, 1592–1596.
- (14) Flick, J.; Ruggenthaler, M.; Appel, H.; Rubio, A. Atoms and Molecules in Cavities, from Weak to Strong Coupling in Quantum-Electrodynamics (QED) Chemistry. *Proc. Natl. Acad. Sci. U. S. A.* **2017**, *114*, 3026–3034.
- (15) Schwartz, T.; Hutchison, J. A.; Léonard, J.; Genet, C.; Haacke, S.; Ebbesen, T. W. Polariton Dynamics under Strong Light–Molecule Coupling. *ChemPhysChem* **2013**, *14*, 125–131.
- (16) Herrera, F.; Spano, F. C. Dark Vibronic Polaritons and the Spectroscopy of Organic Microcavities. *Phys. Rev. Lett.* **2017**, *118*, 223601.
- (17) Martínez-Martínez, L. A.; Du, M.; Ribeiro, R.; Kéna-Cohen, S.; Yuen-Zhou, J. Polariton-Assisted Singlet Fission in Acene Aggregates. *J. Phys. Chem. Lett.* **2018**, *9*, 1951–1957.
- (18) Sanvitto, D.; Kéna-Cohen, S. The Road towards Polaritonic Devices. *Nat. Mater.* **2016**, *15*, 1061–1073.
- (19) Gu, B.; Mukamel, S. Manipulating Two-Photon-Absorption of Cavity Polaritons by Entangled Light. *J. Phys. Chem. Lett.* **2020**, *11*, 8177–8182.
- (20) Gu, B.; Mukamel, S. Manipulating Nonadiabatic Conical Intersection Dynamics by Optical Cavities. *Chem. Sci.* **2020**, *11*, 1290–1298.

- (21) Gu, B.; Mukamel, S. Cooperative Conical Intersection Dynamics of Two Pyrazine Molecules in an Optical Cavity. *J. Phys. Chem. Lett.* **2020**, *11*, 5555–5562.
- (22) Yang, K. Y.; Oh, D. Y.; Lee, S. H.; Yang, Q.-F.; Yi, X.; Shen, B.; Wang, H.; Vahala, K. Bridging Ultrahigh- Q Devices and Photonic Circuits. *Nat. Photonics* **2018**, *12*, 297–302.
- (23) Purcell, E. M. Spontaneous Emission Probabilities at Radio Frequencies. *Phys. Rev.* **1946**, *69*, 681.
- (24) Zhong, X.; Chervy, T.; Zhang, L.; Thomas, A.; George, J.; Genet, C.; Hutchison, J. A.; Ebbesen, T. W. Energy Transfer between Spatially Separated Entangled Molecules. *Angew. Chem., Int. Ed.* **2017**, *56*, 9034–9038.
- (25) George, J.; Shalabney, A.; Hutchison, J. A.; Genet, C.; Ebbesen, T. W. Liquid-Phase Vibrational Strong Coupling. *J. Phys. Chem. Lett.* **2015**, *6*, 1027–1031.
- (26) Benz, F.; Schmidt, M. K.; Dreismann, A.; Chikkaraddy, R.; Zhang, Y.; Demetriadou, A.; Carnegie, C.; Ohadi, H.; de Nijs, B.; Esteban, R.; Aizpurua, J.; Baumberg, J. J. Single-Molecule Optomechanics in "Picocavities. *Science* **2016**, *354*, 726–729.
- (27) Zhong, X.; Chervy, T.; Wang, S.; George, J.; Thomas, A.; Hutchison, J. A.; Devaux, E.; Genet, C.; Ebbesen, T. W. Non-Radiative Energy Transfer Mediated by Hybrid Light-Matter States. *Angew. Chem.* **2016**, *128*, 6310–6314.
- (28) Suzuki, M.; Nishiyama, K.; Kani, N.; Funahashi, M.; Nakanishi, S.; Tsurumachi, N. Dual-Colour Pump-Probe Spectroscopy to Observe the Transition between Polariton Branches in an Ultrastrongly Coupled Microcavity Containing Organic Dye Molecules. *Jpn. J. Appl. Phys.* **2020**, *59*, SCCA08.
- (29) Chikkaraddy, R.; de Nijs, B.; Benz, F.; Barrow, S. J.; Scherman, O. A.; Rosta, E.; Demetriadou, A.; Fox, P.; Hess, O.; Baumberg, J. J. Single-Molecule Strong Coupling at Room Temperature in Plasmonic Nanocavities. *Nature* **2016**, *535*, 127–130.
- (30) Du, M.; Ribeiro, R. F.; Yuen-Zhou, J. Remote Control of Chemistry in Optical Cavities. *Chem.* **2019**, *5*, 1167–1181.
- (31) Gu, B.; Mukamel, S. Optical-Cavity Manipulation of Conical Intersections and Singlet Fission in Pentacene Dimers. *J. Phys. Chem. Lett.* **2021**, *12*, 2052–2056.
- (32) Orgiu, E.; George, J.; Hutchison, J. A.; Devaux, E.; Dayen, J. F.; Doudin, B.; Stellacci, F.; Genet, C.; Schachenmayer, J.; Genes, C.; Pupillo, G.; Samorì, P.; Ebbesen, T. W. Conductivity in Organic Semiconductors Hybridized with the Vacuum Field. *Nat. Mater.* **2015**, *14*, 1123–1129.
- (33) Thomas, A.; Lethuillier-Karl, L.; Nagarajan, K.; Vergauwe, R. M. A.; George, J.; Chervy, T.; Shalabney, A.; Devaux, E.; Genet, C.; Moran, J.; Ebbesen, T. W. Tilting a Ground-State Reactivity Landscape by Vibrational Strong Coupling. *Science* **2019**, *363*, 615–619.
- (34) Xiang, B.; Ribeiro, R. F.; Du, M.; Chen, L.; Yang, Z.; Wang, J.; Yuen-Zhou, J.; Xiong, W. Intermolecular Vibrational Energy Transfer Enabled by Microcavity Strong Light—Matter Coupling. *Science* **2020**, 368, 665—667.
- (35) Ulusoy, I. S.; Gomez, J. A.; Vendrell, O. Modifying the Nonradiative Decay Dynamics through Conical Intersections via Collective Coupling to a Cavity Mode. *J. Phys. Chem. A* **2019**, *123*, 8832–8844.
- (36) Ribeiro, R. F.; Martínez-Martínez, L. A.; Du, M.; Campos-Gonzalez-Angulo, J.; Yuen-Zhou, J. Polariton Chemistry: Controlling Molecular Dynamics with Optical Cavities. *Chem. Sci.* **2018**, *9*, 6325–6339.
- (37) Du, M.; A. Martínez-Martínez, L.; R. Ribeiro, F.; Hu, Z.; M. Menon, V.; Yuen-Zhou, J. Theory for Polariton-Assisted Remote Energy Transfer. *Chem. Sci.* **2018**, *9*, 6659–6669.
- (38) Zhang, Y.; Nelson, T.; Tretiak, S. Non-Adiabatic Molecular Dynamics of Molecules in the Presence of Strong Light-Matter Interactions. *J. Chem. Phys.* **2019**, *151*, 154109.
- (39) Sun, S.; Gu, B.; Mukamel, S. Polariton ring currents and circular dichroism of Mg-porphyrin in a chiral cavity. *Chem. Sci.* **2022**, *13*, 1037–1048.

- (40) Domcke, W.; Yarkony, D. R.; Köppel, H. Conical Intersections: Theory, Computation and Experiment; World Scientific, 2011.
- (41) Lim, J. S.; Kim, S. K. Experimental probing of conical intersection dynamics in the photodissociation of thioanisole. *Nat. Chem.* **2010**, *2*, 627–632.
- (42) You, H. S.; Han, S.; Lim, J. S.; Kim, S. K.  $(\pi\pi^*/\pi\sigma^*)$  Conical Intersection Seam Experimentally Observed in the S–D Bond Dissociation Reaction of Thiophenol- $d_1$ . *J. Phys. Chem. Lett.* **2015**, 6, 3202–3208.
- (43) Musser, A. J.; Liebel, M.; Schnedermann, C.; Wende, T.; Kehoe, T. B.; Rao, A.; Kukura, P. Evidence for conical intersection dynamics mediating ultrafast singlet exciton fission. *Nat. Phys.* **2015**, *11*, 352–357.
- (44) Worner, H. J.; Bertrand, J. B.; Fabre, B.; Higuet, J.; Ruf, H.; Dubrouil, A.; Patchkovskii, S.; Spanner, M.; Mairesse, Y.; Blanchet, V.; Mevel, E.; Constant, E.; Corkum, P. B.; Villeneuve, D. M. Conical Intersection Dynamics in NO2 Probed by Homodyne High-Harmonic Spectroscopy. *Science* **2011**, 334, 208–212.
- (45) Horio, T.; Fuji, T.; Suzuki, Y.-I.; Suzuki, T. Probing Ultrafast Internal Conversion through Conical Intersection via Time-Energy Map of Photoelectron Angular Anisotropy. *J. Am. Chem. Soc.* **2009**, 131, 10392–10393.
- (46) Hoffman, D. P.; Ellis, S. R.; Mathies, R. A. Characterization of a Conical Intersection in a Charge-Transfer Dimer with Two-Dimensional Time-Resolved Stimulated Raman Spectroscopy. *J. Phys. Chem. A* **2014**, *118*, 4955–4965.
- (47) Hoffman, D. P.; Mathies, R. A. Femtosecond Stimulated Raman Exposes the Role of Vibrational Coherence in Condensed-Phase Photoreactivity. *Acc. Chem. Res.* **2016**, 49, 616–625.
- (48) Polli, D.; Altoè, P.; Weingart, O.; Spillane, K. M.; Manzoni, C.; Brida, D.; Tomasello, G.; Orlandi, G.; Kukura, P.; Mathies, R. A.; Garavelli, M.; Cerullo, G. Conical intersection dynamics of the primary photoisomerization event in vision. *Nature* **2010**, *467*, 440–443.
- (49) McFarland, B. K.; et al. Ultrafast X-ray Auger probing of photoexcited molecular dynamics. *Nat. Commun.* **2014**, *5*, 4235.
- (50) Raab, A.; Worth, G. A.; Meyer, H.-D.; Cederbaum, L. S. Molecular dynamics of pyrazine after excitation to the S2 electronic state using a realistic 24-mode model Hamiltonian. *J. Chem. Phys.* **1999**, *110*, 936–946.
- (51) Oliver, T. A. A.; Lewis, N. H. C.; Fleming, G. R. Correlating the motion of electrons and nuclei with two-dimensional electronic-vibrational spectroscopy. *Proc. Natl. Acad. Sci. U.S.A.* **2014**, *111*, 10061–10066.
- (52) Timmers, H.; Li, Z.; Shivaram, N.; Santra, R.; Vendrell, O.; Sandhu, A. Coherent Electron Hole Dynamics Near a Conical Intersection. *Phys. Rev. Lett.* **2014**, *113*, 113003.
- (53) Kowalewski, M.; Mukamel, S. Stimulated Raman signals at conical intersections: Ab initio surface hopping simulation protocol with direct propagation of the nuclear wave function. *J. Chem. Phys.* **2015**, *143*, No. 044117.
- (54) von Conta, A.; Tehlar, A.; Schletter, A.; Arasaki, Y.; Takatsuka, K.; Worner, H. J. Conical-intersection dynamics and ground-state chemistry probed by extreme-ultraviolet time-resolved photoelectron spectroscopy. *Nat. Commun.* **2018**, *9*, 3162.
- (55) Kowalewski, M.; Bennett, K.; Dorfman, K. E.; Mukamel, S. Catching Conical Intersections in the Act: Monitoring Transient Electronic Coherences by Attosecond Stimulated X-Ray Raman Signals. *Phys. Rev. Lett.* **2015**, *115*, 193003.
- (56) Szidarovszky, T.; Halász, G. J.; Császár, A. G.; Cederbaum, L. S.; Vibók, Á. Conical Intersections Induced by Quantum Light: Field-Dressed Spectra from the Weak to the Ultrastrong Coupling Regimes. *J. Phys. Chem. Lett.* **2018**, *9*, 6215–6223.
- (57) Vendrell, O. Coherent Dynamics in Cavity Femtochemistry: Application of the Multi-Configuration Time-Dependent Hartree Method. *Chem. Phys.* **2018**, *509*, 55.
- (58) Xiang, B.; Ribeiro, R. F.; Dunkelberger, A. D.; Wang, J.; Li, Y.; Simpkins, B. S.; Owrutsky, J. C.; Yuen-Zhou, J.; Xiong, W. Two-

- Dimensional Infrared Spectroscopy of Vibrational Polaritons. *Proc. Natl. Acad. Sci. U.S.A.* **2018**, *115*, 4845–4850.
- (59) Avramenko, A. G.; Rury, A. S. Local Molecular Probes of Ultrafast Relaxation Channels in Strongly Coupled Metalloporphyrin-Cavity Systems. *J. Chem. Phys.* **2021**, *155*, No. 064702.
- (60) Saurabh, P.; Mukamel, S. Two-Dimensional Infrared Spectroscopy of Vibrational Polaritons of Molecules in an Optical Cavity. *J. Chem. Phys.* **2016**, *144*, 124115.
- (61) Cho, M. Coherent Two-Dimensional Optical Spectroscopy. Chem. Rev. 2008, 108, 1331–1418.
- (62) Mukamel, S. Principles of Nonlinear Optical Spectroscopy; Oxford University Press, 1995.
- (63) Seidner, L.; Stock, G.; Sobolewski, A. L.; Domcke, W. Ab Initio Characterization of the S1–S2 Conical Intersection in Pyrazine and Calculation of Spectra. *J. Chem. Phys.* **1992**, *96*, 5298–5309.
- (64) Domcke, W., Yarkony, D., Köppel, H., Eds. *Conical Intersections: Electronic Structure, Dynamics & Spectroscopy*; Advanced Series in Physical Chemistry v.15; World Scientific: River Edge, NJ, 2004.
- (65) Scheurer, C.; Mukamel, S. Magnetic Resonance Analogies in Multidimensional Vibrational Spectroscopy. *Bull. Chem. Soc. Jpn.* **2002**, 75, 989–999.
- (66) Seidner, L.; Stock, G.; Domcke, W. Nonperturbative approach to femtosecond spectroscopy: General theory and application to multidimensional nonadiabatic photoisomerization processes. *J. Chem. Phys.* **1995**, *103*, 3998–4011.
- (67) Gelin, M. F.; Egorova, D.; Domcke, W. Efficient Calculation of Time- and Frequency-Resolved Four-Wave-Mixing Signals. *Acc. Chem. Res.* **2009**, 42, 1290–1298.
- (68) Hamm, P.; Zanni, M. Concepts and Methods of 2D Infrared Spectroscopy; Cambridge University Press: Cambridge, 2011.
- (69) Krčmář, J.; Gelin, M. F.; Egorova, D.; Domcke, W. Signatures of conical intersections in two-dimensional electronic spectra. *J. Phys. B: At. Mol. Opt. Phys.* **2014**, 47, 124019.
- (70) Krčmář, J.; Gelin, M. F.; Domcke, W. Simulation of femtosecond two-dimensional electronic spectra of conical intersections. *J. Chem. Phys.* **2015**, *143*, No. 074308.
- (71) Sun, K.; Xu, Q.; Chen, L.; Gelin, M. F.; Zhao, Y. Temperature effects on singlet fission dynamics mediated by a conical intersection. *J. Chem. Phys.* **2020**, *153*, 194106.